

# SANDIA REPORT

2015-11134

Unlimited Release

Printed December 2015

## Compressible degree of freedom (CDOF): A potential strategy for improving wave energy capture

Giorgio Bacelli, Vincent S. Neary and Andrew W. Murphy

Prepared by

Sandia National Laboratories

Albuquerque, New Mexico 87185 and Livermore, California 94550

Sandia National Laboratories is a multi-program laboratory managed and operated by Sandia Corporation, a wholly owned subsidiary of Lockheed Martin Corporation, for the U.S. Department of Energy's National Nuclear Security Administration under contract DE-AC04-94AL85000.

Approved for public release; further dissemination unlimited.



**Sandia National Laboratories**

Issued by Sandia National Laboratories, operated for the United States Department of Energy by Sandia Corporation.

**NOTICE:** This report was prepared as an account of work sponsored by an agency of the United States Government. Neither the United States Government, nor any agency thereof, nor any of their employees, nor any of their contractors, subcontractors, or their employees, make any warranty, express or implied, or assume any legal liability or responsibility for the accuracy, completeness, or usefulness of any information, apparatus, product, or process disclosed, or represent that its use would not infringe privately owned rights. Reference herein to any specific commercial product, process, or service by trade name, trademark, manufacturer, or otherwise, does not necessarily constitute or imply its endorsement, recommendation, or favoring by the United States Government, any agency thereof, or any of their contractors or subcontractors. The views and opinions expressed herein do not necessarily state or reflect those of the United States Government, any agency thereof, or any of their contractors.

Printed in the United States of America. This report has been reproduced directly from the best available copy.

Available to DOE and DOE contractors from  
U.S. Department of Energy  
Office of Scientific and Technical Information  
P.O. Box 62  
Oak Ridge, TN 37831

Telephone: (865) 576-8401  
Facsimile: (865) 576-5728  
E-Mail: [reports@adonis.osti.gov](mailto:reports@adonis.osti.gov)  
Online ordering: <http://www.osti.gov/bridge>

Available to the public from  
U.S. Department of Commerce  
National Technical Information Service  
5285 Port Royal Rd  
Springfield, VA 22161

Telephone: (800) 553-6847  
Facsimile: (703) 605-6900  
E-Mail: [orders@ntis.fedworld.gov](mailto:orders@ntis.fedworld.gov)  
Online ordering: <http://www.ntis.gov/help/ordermethods.asp?loc=7-4-0#online>



# Compressible degree of freedom (CDOF): A potential strategy for improving wave energy capture

Giorgio Bacelli<sup>1</sup>, Vincent S. Neary<sup>2</sup>, Andrew W. Murphy<sup>3</sup>

Water Power Technologies Department<sup>1,2</sup>,

Mech Design, Model & Analysis<sup>3</sup>

Sandia National Laboratories

P.O. Box 5800

Albuquerque, NM 87185 - MS1124<sup>1,2</sup> MS0374<sup>3</sup>

gbacell@sandia.gov<sup>1</sup>, vsneary@sandia.gov<sup>2</sup>, awmurph@sandia.gov<sup>3</sup>

## Abstract

The addition of a compressible degree of freedom (CDOF) to a wave energy converter (WEC), resulting in a compressible WEC, has been shown to significantly increase the power absorption compared to a rigid WEC of the same shape and mass for a variety of architectures. The present study demonstrates that a compressible point absorber, with a passive power-take-off (PTO) and optimized damping, can also achieve at the same performance levels or better than an optimally controlled rigid point absorber using reactive power from the PTO. Eliminating the need for a reactive PTO would substantially reduce costs by reducing PTO design complexity. In addition, it would negate the documented problems of reactive PTO efficiencies on absorbed power. Improvements to performance were quantified in the present study by comparing a compressible point absorber to a conventional rigid one with the same shape and mass. Wave energy is converted to mechanical energy in both cases using a linear damper PTO, with the PTO coefficient optimized for each resonance frequency and compressible volume. The large compressible volumes required to tune the compressible point absorber to the desired frequency are a practical limitation that needs to be addressed with further research; especially for low frequencies. In fact, all compressible volumes exceed the submerged volume of the point absorber by significant amounts; requiring auxiliary compressible volume storage units that are connected to the air chamber in

the submerged portion of the point absorber. While realistic, these auxiliary units would increase the CapEx and OpEx costs, potentially reducing the aforementioned benefits gained by CDOF. However, alternative approaches can be developed to implement CDOF without the large compressible volume requirements, including the development of flexible surface panels tuned with mechanical springs.

# Acknowledgment

This study was supported by the Wind and Water Power Technologies Office of the U.S. Department of Energy, Office of Energy Efficiency and Renewable Energy. Sandia National Laboratories is a multi-program laboratory managed and operated by Sandia Corporation, a wholly owned subsidiary of Lockheed Martin Corporation, for the U.S. Department of Energy's National Nuclear Security Administration under contract DE-AC04-94AL85000. The authors are grateful to Dr. Adi Kurniawan and Dr. Deborah Greaves, of the University of Plymouth, who generously responded to questions on their modeling work; as well as Dr. Robert C. Haberman, who derived alternative stiffness terms considering the absolute displacement of the CDOF moving surface.



# Contents

- 1 Introduction** **13**
  
- 2 Heaving Motion of a Rigid Cylinder in Regular Waves** **15**
  - 2.1 One DOF Frequency-Domain Model 15
    - 2.1.1 Hydrostatic and gravity forces 15
    - 2.1.2 Hydrodynamic forces 15
    - 2.1.3 Equation of motion 16
  - 2.2 One DOF Time-Domain Model 17
  
- 3 Modeling Compressible Point Absorbers** **19**
  - 3.1 Heaving Motion of Emergent Compressible Cylinder in Regular Waves 19
    - 3.1.1 Generalized Body Mode Model 20
    - 3.1.2 Two-body model 21
    - 3.1.3 Derivation of stiffness terms for two-body model 22
  - 3.2 Governing Parameters and Limitations 23
  - 3.3 Power-Take-Off models 24
    - 3.3.1 Wells Air Turbine PTO 25
    - 3.3.2 Linear damper PTO between oscillating-body and fixed reference 26
      - 3.3.2.1 Derivation of the optimal PTO impedance 27
      - 3.3.2.2 Analytical verification of optimal damping for stiff compression 29
    - 3.3.3 Power absorption through the relative motion between the oscillating body and the compressible surface 31
      - 3.3.3.1 Derivation of the optimal PTO impedance 31

3.4 Available power density and absorption width .....	33
<b>4 Model-to-Model Comparison</b>	<b>35</b>
<b>5 Optimized PTO Heave and Absorption Width</b>	<b>39</b>
5.1 Compressible point absorber reacting against a fixed reference .....	39
5.2 Self-reacting Point Absorber .....	44
<b>6 Conclusions</b>	<b>47</b>
<b>References</b>	<b>49</b>



# List of Figures

3.1	Emergent compressible heaving cylinder adapted from Fig. 1a in [8] (2014) and [5]. Note that the blue dot represents the center of gravity. . . . .	19
3.2	PTO configuration for compressible point absorber reacting against a fixed reference . . . . .	27
3.3	Self-reacting point absorber . . . . .	31
4.1	Model to model comparison for response of heaving compressible cylinder test cases with varying compressible volumes compared to rigid cylinder. . . . .	36
4.2	Model to model comparison for response of heaving point absorber test cases with varying compressible volumes. . . . .	37
4.3	Model to model comparison for energy capture of heaving point absorber test cases with varying compressible volumes. The theoretical maximum energy capture width is $\lambda/2\pi$ . . . . .	37
4.4	Model to model comparison for response of heaving point absorber test cases comparing rigid absorber with linear damper PTO to compressible absorber with Wells turbine PTO, and compressible absorber with linear damper PTO. . . . .	38
4.5	Model to model comparison for energy capture of heaving point absorber test cases comparing rigid point absorber with linear damper PTO to compressible absorber with Wells turbine PTO, and compressible absorber with linear damper PTO. The theoretical maximum energy capture width is $\lambda/2\pi$ . . . . .	38
5.1	Average absorbed power as function of the wave period for waves with amplitude $A = 1m$ . . . . .	40
5.2	Peak power flowing through the PTO as function of the wave period for waves with amplitude $A = 1m$ . . . . .	41
5.3	Time profile of the power flowing through the PTO for an incident wave with period $T = 8.1s$ and amplitude $A = 1m$ . . . . .	41
5.4	Response Amplitude Operator (RAO) of the WEC and compressible surface . . . . .	43
5.5	Average absorbed power as function of the wave period for waves with amplitude $A = 1m$ . . . . .	44

5.6	Peak power through the PTO as function of the wave period for waves with amplitude $A = 1m$ .....	45
5.7	Time profile of the power flowing through the PTO for an incident wave with period $T = 8s$ and amplitude $A = 1m$ .....	45
5.8	Response Amplitude Operator (RAO) of the WEC and compressible surface .	46
5.9	Comparison of capture ratios, defined as absorbed power divided by available power in eq. (3.64) .....	46

# List of Tables

4.1 Test cases for model-to-model comparison ..... 36



# Chapter 1

## Introduction

The benefits of a compressible degree of freedom (CDOF) for damping structural motions through fluid-structure coupling have been investigated by NASA [5]. More recently, university researchers in the United Kingdom (UK) [8] applied frequency domain models to investigate the benefits of CDOF for wave energy conversion. In their models, they implemented the CDOF by incorporating an air spring with a moving surface at the air-water interface that oscillates vertically at a given frequency of motion. Although their model results were not validated with experimental measurements, they indicate that a CDOF could be used in various WEC configurations to improve the body response and power performance. For compressible emergent heaving WECs, the models predicted that the CDOF lowered the resonance frequency compared to a rigid WEC of equal dimensions. Compressible submerged stationary WECs with upward-facing moving surfaces significantly broadened the resonance bandwidth, and achieved 80% of the theoretical maximum power absorption over a wave period range of about 4 seconds.

The Wind and Water Power Technologies Office (WWPTO), of the U.S. Department of Energy (USDOE), is specifically interested in the potential benefits of CDOF for emergent compressible WECs, e.g., the compressible wave point absorbers examined by [8]. These benefits were found to be less impactful compared to the simple bed mounted WEC with an air turbine PTO. However, the UK study was limited to point absorbers with simple linear damper PTOs that were suboptimal. This study also did not examine how the CDOF could be further exploited using passive phase control.

The present study reviews the equations of motion and terms for modeling the CDOF effects in the frequency domain, based on work by [8], [5], and [6]. Its scope is limited to compressible heaving point absorbers, beginning with a one-degree-of-freedom (1 DOF) rigid cylinder, which serves as a baseline for comparison. It then reviews the equations of motion for the 2 DOF compressible emergent heaving cylinder investigated in the UK study [8]. An alternative derivation of the stiffness terms is carried out to verify those derived in the UK study. In addition, independently derived numerical models are developed, and results from these models compared to those from the UK study [8]. Several test cases are considered, including one for the heaving compressible cylinder case and several test cases that consider emergent WECs with CDOF and power-take-offs. The present study extends the work of [8] by developing an optimized power-take-off (PTO) model, and considering a self-reacting point absorber, as well as one that reacts to a fixed reference.



# Chapter 2

## Heaving Motion of a Rigid Cylinder in Regular Waves

The governing equation for the heaving motion of a heaving rigid cylinder subject to a free decay test is presented by [7]. It is adapted here to develop the equation of motion in the time and frequency domain for a heaving rigid cylinder of radius  $r$  and draught,  $d$ . All subsequent equations assume the heaving cylinder is excited by regular ocean swell waves with periods on the order of ten seconds.

### 2.1 One DOF Frequency-Domain Model

#### 2.1.1 Hydrostatic and gravity forces

At static equilibrium, the weight of the cylinder  $W$  in the fluid is equal to the buoyancy force

$$W = B = \rho g a d = \rho g \pi r^2 d \quad (2.1)$$

Where  $\rho$  is the density of the fluid (e.g., saltwater,  $\rho = 1025 \text{ kg/m}^3$ ),  $g = 9.806 \text{ m/s}^2$  is the gravitational constant,  $a = \pi r^2$  is the water plane area, and  $d$  is the draught (submerged depth).

If the cylinder is displaced upward vertically a distance  $\xi$  from the water surface, the difference between the cylinders weight and its buoyancy force is the hydrostatic restoring force (i.e., the force that restores the body back to its static equilibrium), where

$$F_{hs} = \rho g a (d - \xi) - \rho g A d = \rho g a \xi \quad (2.2)$$

is a spring force with a stiffness or restoring spring constant equal to  $\rho g a$  ( $N/m = \text{kg/s}^2$ ).

#### 2.1.2 Hydrodynamic forces

The model for the wave-body interaction used in the present study is based on linear potential theory [3]. Using this framework, the forces acting on a body floating due to the

interaction with the fluid result from the linearization with respect to two variables, which are the velocity of the floating body and the amplitude of the sinusoidal incident wave. The response to more complex types of wave spectra is generally modeled using the principle of superposition, that is from the linear combination of the responses to a number of sinusoidal (harmonic) waves.

The time profile  $\eta(t)$  of a sinusoidal wave oscillating at a frequency  $\omega$  can be described, at a specific location (e.g.  $x = 0$ ), using the complex amplitude  $\hat{A}$  as

$$\eta(t) = \text{Re} \left\{ \hat{A} e^{i\omega t} \right\} \quad (2.3)$$

The linearized hydrodynamic forces acting on a floating body subject to a sinusoidal incident wave as in eq. (2.3), can be described as the contribution of two terms, a radiation force ( $F_r$ ) which is proportional to the velocity of the body, and an excitation force ( $F_e$ ) which is proportional to the amplitude of the incident wave as

$$\hat{F}_{hd} = \hat{F}_r + \hat{F}_e = -Z_r \hat{u} + H_e \hat{A} \quad (2.4)$$

where  $\hat{u}$  is the complex amplitude of the body velocity, related to the displacement  $\hat{\xi}$  as  $\hat{u} = i\omega\hat{\xi}$ ;  $Z_r$  is the (frequency dependent) radiation impedance matrix and  $H_e$  is the (complex and frequency dependent) vector of the excitation force coefficients. The radiation impedance  $Z_r$  is generally written explicitly using the real and imaginary parts as

$$Z_r(\omega) = R(\omega) + i\omega m(\omega) \quad (2.5)$$

where  $R$  is the radiation damping and  $m$  is the added mass. Both the radiation impedance matrix and the excitation force coefficients are calculated using boundary element method software, e.g., WAMIT [2], NEMOH [1]. These coefficients are typically normalized, where the excitation force coefficient is the excitation force per unit amplitude divided by the fluid density and gravity, the added mass coefficient is the added mass divided by fluid density, and the radiation damping coefficient is the radiation damping divided by the fluid density and angular velocity.

### 2.1.3 Equation of motion

The motion of the cylinder can be described by using Newton's second law. The forces acting on the body are the hydrostatic force ( $F_{hs}$ ) in (2.2) and the hydrodynamic force ( $F_{hd}$ ) in (2.4), thus

$$\hat{F}_e + \hat{F}_r + \hat{F}_{hs} = (i\omega)^2 \hat{\xi} M. \quad (2.6)$$

Substituting (2.2) and (2.4), (2.6) can be expressed as

$$\hat{F}_e = [(i\omega)^2 (M + m(\omega)) + i\omega R(\omega) + \rho g a] \hat{\xi} \quad (2.7)$$

The equation of motion in (2.7) has been obtained using linear potential theory, and it is valid under the assumptions given by Yu and Falnes [11]: small displacements, neglects friction, and that body motion in waves can be modeled by superimposing the forces due to its motion in still water with the wave excitation force when it is restrained.



## 2.2 One DOF Time-Domain Model

The time-domain model is derived by taking the inverse Fourier transform of the frequency domain model in (2.7)<sup>1</sup>, the result of which is:

$$(M + m_\infty) \ddot{\xi}(t) + \int_0^t k(t - \tau) \dot{\xi}(\tau) d\tau + \rho g a \xi(t) = \int_{-\infty}^{+\infty} h(t - \tau) \eta(\tau) d\tau. \quad (2.8)$$

The excitation impulse response  $h(t)$  function is the inverse Fourier transform of the excitation force coefficient, that is

$$h(t) = \mathcal{F}^{-1} \{H_e(\omega)\} = \frac{1}{2\pi} \int_{-\infty}^{+\infty} H_e(\omega) e^{i\omega t} d\omega. \quad (2.9)$$

It is known that the impulse response  $h(t)$  is non-causal [11], that is  $h(t) \neq 0$  for  $t < 0$ ; however, this is a mathematical artifact that does not, in general, affect the simulation of the WEC. In fact, the excitation force depends only on the time profile of the wave elevation, and it does not depend on the motion of the floating body; therefore, the excitation force can be pre-computed before the simulation is started.

The calculation of the radiation impulse response function is not as straightforward as for the excitation force impulse response. In fact, the radiation impedance is, in general, not integrable because

$$\lim_{\omega \rightarrow +\infty} m(\omega) = m_\infty \neq 0. \quad (2.10)$$

To obviate this issue, the inverse Fourier transform is carried out as

$$\mathcal{F}^{-1} \{Z_r(\omega) u(\omega)\} = \mathcal{F}^{-1} \{(Z_r(\omega) + i\omega m_\infty - i\omega m_\infty) u(\omega)\} \quad (2.11)$$

$$= \mathcal{F}^{-1} \{(R(\omega) + i\omega (m(\omega) - m_\infty) + i\omega m_\infty) u(\omega)\} \quad (2.12)$$

$$= \frac{1}{2\pi} \int_{-\infty}^{+\infty} (R(\omega) + i\omega (m(\omega) - m_\infty) + i\omega m_\infty) u(\omega) e^{i\omega t} d\omega \quad (2.13)$$

$$= \frac{1}{2\pi} \int_{-\infty}^{+\infty} (R(\omega) + i\omega (m(\omega) - m_\infty) + i\omega m_\infty) u(\omega) e^{i\omega t} d\omega \quad (2.14)$$

$$= \int_0^t k(t - \tau) \dot{\xi}(\tau) d\tau + m_\infty \ddot{\xi}(t) \quad (2.15)$$

where  $u(\omega)$  is the velocity in the frequency domain, that is  $\mathcal{F}\{\dot{\xi}(t)\} = u(\omega)$ , and where the last step has been carried out by exploiting the fact that the impulse response function  $k(t)$

---

<sup>1</sup>In reality, it is not rigorously exact to take the inverse Fourier transform of eq. (2.7), as the variables (force and displacement) are complex amplitudes. In order for the derivation to be rigorous, these quantities should be considered as variables in the frequency domain instead of complex amplitudes, that is,  $\hat{\xi}$  should be replaced with  $\xi(\omega) = \mathcal{F}\{\xi(t)\}$  and  $\hat{F}_e$  should be replaced  $F_e(\omega) = \mathcal{F}\{F_e(t)\}$ .

must be real, thus the Ogilvie relations [10] hold:

$$R(\omega) = \int_0^{\infty} k(t) \cos(\omega t) dt \quad (2.16)$$

$$m(\omega) = m_{\infty} - \frac{1}{\omega} \int_0^{\infty} k(t) \sin(\omega t) dt. \quad (2.17)$$

# Chapter 3

## Modeling Compressible Point Absorbers

### 3.1 Heaving Motion of Emergent Compressible Cylinder in Regular Waves

The 2 DOF emergent compressible heaving cylinder investigated in the UK study [8] is illustrated in Figure 3.1. It has an air chamber in the submerged portion of the cylinder. This air chamber is connected to a circular moving surface at the bottom of the cylinder that acts as an air spring that oscillates vertically at a given frequency of motion. The following sections review alternative equations of motion for this case, those in which the moving surface is modeled as a Generalized Body Mode (GBM), the approach in [8], and those where the moving surface is modeled as a separate body, the two-body model. The comparison allows an independent verification of the stiffness terms, detailed in the section below.

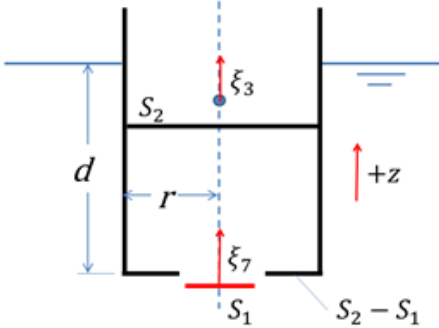


**Figure 3.1.** Emergent compressible heaving cylinder adapted from Fig. 1a in [8] (2014) and [5]. Note that the blue dot represents the center of gravity.

### 3.1.1 Generalized Body Mode Model

The approach taken by [8] was to model the moving surface as a generalized body mode. The equations of motion are expressed in state-space form as

$$\left( -\omega^2 \begin{bmatrix} M + m_{33} & m_{37} \\ m_{73} & m_{77} \end{bmatrix} + i\omega \begin{bmatrix} R_{33} & R_{37} \\ R_{73} & R_{77} \end{bmatrix} + \begin{bmatrix} k_{33} & k_{37} \\ k_{73} & k_{77} \end{bmatrix} \right) \begin{bmatrix} \xi_3 \\ \xi_r \end{bmatrix} = \begin{bmatrix} F_{e3} \\ F_{e7} \end{bmatrix} \quad (3.1)$$

In this formulation, the moving surface is assumed to have zero mass<sup>1</sup>, and  $M$  is the mass of the cylinder (body 1) with water plane area  $S_2$ . The displacement for body 1, denoted by  $\xi_3$ , is relative to a fixed reference point at its center of gravity at static equilibrium. The moving surface has zero mass, and area  $S_1$ . Its displacement is relative to the cylinder because it is modeled as a generalized body mode in the radiation-diffraction model, not as a separate body; where  $\xi_r = \xi_7 - \xi_3$ , and  $\xi_7$  represents the absolute heave displacement, i.e., the displacement of the moving surface relative to a fixed reference at the bottom of the cylinder at static equilibrium. The positive z-direction is upwards to coincide with the unit normal vector on the moving surface, which points into the air chamber.

As for the rigid cylinder case, coefficients needed to determine the excitation force amplitude and phase angle, added mass terms,  $m_{ij}$ , and the radiation damping terms,  $R_{ij}$ , are derived from a radiation-diffraction model, e.g., WAMIT [2], NEMOH [1]. Because the moving surface is modeled as a generalized body mode [9], these terms, as well as the stiffness terms,  $K_{ij}$ , assume the excitation force,  $F_{e3}$ , acts on body 1 (the cylinder and moving surface), and the displacement of the moving surface is relative to the cylinder.

As shown by [8], the stiffness terms for the GBM model,  $K_{ij}$ , are

$$\begin{bmatrix} k_{33} & k_{37} \\ k_{73} & k_{77} \end{bmatrix} = \begin{bmatrix} \rho g S_2 & \rho g S_1 \\ \rho g S_1 & \rho g S_1 + \frac{\gamma p_0}{v_0} S_1^2 \end{bmatrix} \quad (3.2)$$

These stiffness terms are spring constants for the restoring forces acting on body 1 and the moving surface. For heaving solid bodies, restoring forces are only due to hydrostatic pressure changes caused by displacement. But the pneumatic force acting on the moving surface, due to pressure changes of the compressible volume, needs to be included when modeling the CDOF. The net pneumatic force acting on body 1 is zero because the area of the ceiling of the chamber  $S_2$  is equal to the sum of the area of the moving surface,  $S_1$ , and the area of the bottom of the cylinder,  $S_2 - S_1$ . The hydrostatic restoring forces act on body 1 include the component due to the displacement of body 1,  $-K_{33}\xi_3 = -\rho g S_2 \xi_3$ , and that due to the displacement of the moving surface relative to body 1,  $-K_{37}\xi_r = -\rho g S_1 \xi_r$ . The stiffness term  $K_{73} = \rho g S_1$  because a downward displacement of body 1 by  $\xi_3$  generates an upward hydrostatic restoring force acting on the moving surface,  $-K_{73}\xi_3 = -\rho g S_1 \xi_3$ .

---

<sup>1</sup>In practice, it is assumed that  $M_s$ , the mass of the moving surface, is such that  $M_s \ll M, m_{37}, m_{73}, m_{77}$ , thus  $M + M_s \approx M$ ,  $m_{37} + M_s \approx m_{37}$ ,  $m_{73} + M_s \approx m_{73}$ ,  $m_{77} + M_s \approx m_{77}$ .

Similarly, a downward displacement of the moving surface relative to body 1 generates an upward hydrostatic restoring force,  $-\rho g S_1 \xi_r$ . An additional downward pneumatic force acts on the area of the moving surface,  $S_1$ , due to the pressure change in the chamber, and must be added to the hydrostatic restoring force as shown in (3.2). Details on the derivation of this pneumatic force term are given in [8].

### 3.1.2 Two-body model

An alternative formulation treats the cylinder and moving surface in Figure 3.1 as two separate bodies, where the excitation force,  $\bar{F}_{e3} = F_{e3} - F_{e7}$ , acts only on the cylinder. Substituting this relation into (3.1), the equations of motion become

$$\left( \begin{array}{cc} -\omega^2 \begin{bmatrix} M + m_{33} - m_{73} & m_{37} - m_{77} \\ m_{73} & m_{77} \end{bmatrix} + i\omega \begin{bmatrix} R_{33} - R_{73} & R_{37} - R_{77} \\ R_{73} & R_{77} \end{bmatrix} \\ + \begin{bmatrix} k_{33} - k_{73} & k_{37} - k_{77} \\ k_{73} & k_{77} \end{bmatrix} \end{array} \right) \begin{bmatrix} \xi_3 \\ \xi_r \end{bmatrix} = \begin{bmatrix} \bar{F}_{e3} \\ F_{e7} \end{bmatrix} \quad (3.3)$$

Substituting  $\xi_r = \xi_7 - \xi_3$ , the equations of motion for the two body model with absolute displacement of the moving surface becomes

$$\left( \begin{array}{cc} -\omega^2 \begin{bmatrix} M + m_{33} - m_{73} - (m_{37} - m_{77}) & m_{37} - m_{77} \\ m_{73} - m_{77} & m_{77} \end{bmatrix} \\ + i\omega \begin{bmatrix} R_{33} - R_{73} - (R_{37} - R_{77}) & R_{37} - R_{77} \\ R_{73} - R_{77} & R_{77} \end{bmatrix} \\ + \begin{bmatrix} k_{33} - k_{73} - (k_{37} - k_{77}) & k_{37} - k_{77} \\ k_{73} - k_{77} & k_{77} \end{bmatrix} \end{array} \right) \begin{bmatrix} \xi_3 \\ \xi_7 \end{bmatrix} = \begin{bmatrix} \bar{F}_{e3} \\ F_{e7} \end{bmatrix} \quad (3.4)$$

Therefore, the stiffness terms in the two body model are

$$\begin{bmatrix} k_{33} - k_{73} - (k_{37} - k_{77}) & k_{37} - k_{77} \\ k_{73} - k_{77} & k_{77} \end{bmatrix} = \begin{bmatrix} \rho g (S_2 - S_1) & -\frac{\gamma p_0}{v_0} S_1^2 \\ -\frac{\gamma p_0}{v_0} S_1^2 & \rho g S_1 + \frac{\gamma p_0}{v_0} S_1^2 \end{bmatrix} \quad (3.5)$$

These terms are derived in the following section as an independent verification of those in the GBM model.

### 3.1.3 Derivation of stiffness terms for two-body model

Terms in the stiffness matrix,  $K_{ij}$ , are derived following [6] with the displacement positive in the upward direction as illustrated in Figure 3.1. The restoring forces include the hydrostatic forces due to depth changes, and the pneumatic forces due to changes in the internal pressures acting on both bodies. Assuming the cylinder body (body 1) and the CDOF moving surface (body 2) are displaced upwards in the positive z-direction a distance  $\xi_3$  and  $\xi_7$ , the hydrostatic forces on each surface are reduced by

$$F_{b_3} = -\rho g (S_2 - S_1) \xi_3 \quad \text{and} \quad F_{b_7} = -\rho g S_1 \xi_7 \quad (3.6)$$

The net pneumatic force acting on the cylinder due to the pressure change  $p$  in the chamber is

$$F_{p_a} = pS_2 - p(S_2 - S_1) = pS_1 \quad (3.7)$$

where the first term on the right hand side is acting on the ceiling of the chamber, and the second term acts on the floor surrounding the moving surface. The net pneumatic force acting on the moving surface is

$$F_{p_7} = -pS_1 \quad (3.8)$$

The signs indicate that the pneumatic force on the cylinder acts upwards, while that on the moving surface acts downwards.

The relationship between the pressure change and the relative displacement is derived by substituting the definition for a positive volume change

$$v = S_1 (\xi_3 - \xi_7) = -S_1 (\xi_7 - \xi_3) \quad (3.9)$$

into the linearized pressure-volume relationship

$$p = -\frac{\gamma p_0}{v_0} v \quad (3.10)$$

resulting in

$$p = \frac{\gamma p_0}{v_0} S_1 (\xi_7 - \xi_3) \quad (3.11)$$

where

$$p_0 = \text{equilibrium pressure at moving surface (Pa)} \quad (3.12)$$

$$v_0 = \text{equilibrium air volume (m}^3\text{)} \quad (3.13)$$

$$v = \text{positive change in volume (m}^3\text{) requires } \xi_3 > \xi_7 \quad (3.14)$$

$$\gamma = \text{adiabatic index (1.4 for air)} \quad (3.15)$$

$$(3.16)$$

Substitution of the pressure relationship into the pneumatic force terms and combining the hydrostatic force terms leads to

$$F_{K_3} = \left( -\rho g (S_2 - S_1) - \frac{\gamma p_0}{v_0} S_1^2 \right) \xi_3 + \left( \frac{\gamma p_0}{v_0} S_1^2 \right) \xi_7 \quad (3.17)$$

$$F_{K_7} = \left( \frac{\gamma p_0}{v_0} S_1^2 \right) \xi_3 + \left( -\rho g S_1 - \frac{\gamma p_0}{v_0} S_1^2 \right) \xi_7 \quad (3.18)$$

Noting that the spring constant is negative, the stiffness matrix in the state space equation becomes

$$\begin{bmatrix} k_{33} - k_{73} - (k_{37} - k_{77}) & k_{37} - k_{77} \\ k_{73} - k_{77} & k_{77} \end{bmatrix} = \begin{bmatrix} \rho g (S_2 - S_1) & -\frac{\gamma p_0}{v_0} S_1^2 \\ -\frac{\gamma p_0}{v_0} S_1^2 & \rho g S_1 + \frac{\gamma p_0}{v_0} S_1^2 \end{bmatrix} \quad (3.19)$$

which is in agreement with (3.5) and indicates that the stiffness terms in both models are consistent with one another.

## 3.2 Governing Parameters and Limitations

The CDOF in an emergent heaving compressible cylinder is effectively an air spring, with a spring constant that depends on the surface area,  $S_1$ , of the moving surface, the initial compressible volume of air in the chamber,  $v_0$ , and the initial pressure on the moving surface,  $p_0$ , which depends on its submerged depth,  $d$ .

For the emergent heaving compressible cylinder, the design natural frequency of the cylinder body was shown by [8] to be

$$\omega_{n_3} = \sqrt{\frac{\rho g (S_2 + S_1 r)}{M + m_{33} + m_{37} r}} \quad (3.20)$$

where

$$r = -\frac{\rho g}{S_1 \frac{\gamma p_0}{v_0} + \rho g}. \quad (3.21)$$

It has to be noted that the expression describing the resonance frequency in (3.20) is an approximation, which is obtained by neglecting the inertia associated with the mass of the moving surface and the fluid mass  $m_{77}$ ; additionally, it is also assumed that the frequency dependence of the mass terms  $m_{ij}$  is small.

However, the formula in (3.20) is still useful to provide insight on the parameters affecting the resonance frequency (i.e. the tuning of the device). More specifically, since  $S_1, p_0$  and  $v_0$  are positive, the bounds on the ratio  $r$  are

$$-1 \leq r \leq 0. \quad (3.22)$$

The upper bound on the resonance frequency can be obtained by taking the following limit:

$$\lim_{v_0 \rightarrow 0} r = 0 \quad \implies \quad \lim_{v_0 \rightarrow 0} \omega_{n_3} = \sqrt{\frac{\rho g S_2}{M + m_{33}}} \quad (3.23)$$

that is, when the compressible volume goes to zero then the resonance frequency is the same as the resonance frequency of the rigid body. Additionally,

$$\lim_{v_0 \rightarrow \infty} r = -1 \quad \implies \quad \lim_{v_0 \rightarrow \infty, S_1 \rightarrow S_2} \omega_{n_3} = 0. \quad (3.24)$$

Therefore, assuming  $S_1 \leq S_2$ , the bounds of the natural frequency in heave are:

$$0 \leq \omega_{n_3} \leq \sqrt{\frac{\rho g S_2}{M + m_{33}}}. \quad (3.25)$$

### 3.3 Power-Take-Off models

Wave power conversion to mechanical power is simulated using three different power take-off (PTO) models: A Wells air turbine, which is driven by air flow exchange between the compressible volume on the device and a fixed volume in an auxiliary chamber; A linear damper PTO; and a linear spring damper PTO. The equations for calculating the absorbed power for each of these PTO models, and those for calculating the available wave power density and absorption width, are described in the following sections.



### 3.3.1 Wells Air Turbine PTO

The governing equations and implementation of the Wells turbine PTO model are described in the UK study [8]. The mass flow rate through the Wells turbine, in units  $kg/s$ , is approximated as

$$i\omega m_2 = -i\omega m_1 = C(p_1 - p_2) \quad (3.26)$$

where  $C$  [ $ms$ ] is the turbine coefficient,  $m_1$  [ $kg$ ] is the change of air mass in the compressible volume,  $m_2$  [ $kg$ ] is the change in air mass in the fixed volume,  $p_1$  [ $Pa = N/m^2$ ] is the change in dynamic pressure of the compressible volume, and  $p_2$  [ $Pa = N/m^2$ ] is the change in dynamic pressure of the fixed volume. Using this relationship, and (4.1) from [8], the frequency dependent variable  $D$  may be defined as

$$D = \frac{C}{\gamma p_o C + i\omega m_{20}} \quad (3.27)$$

where  $m_{20}$  [ $kg$ ] is the equilibrium mass of the fixed volume. Following the derivation in [8], a complex non-dimensional quantity  $L$  relates the pneumatic force on the moving surface to the restoring force from the turbine and fixed volumes. The non-dimensional quantity  $L$  is defined as

$$L \equiv \frac{S_1}{\rho g V_{10} \left( \left( \frac{m_{20}}{m_{10}} \right) D + \frac{1}{\gamma p_o} \right)} \quad (3.28)$$

where the complex portion of  $L$  is proportional to the moving surface velocity and the real part of  $L$  is proportional to its displacement. These terms are added to the  $R_{77}$  and  $K_{77}$  terms of (3.1). When the turbine coefficient,  $C$ , goes to zero, the equation of motion for the compressible heaving cylinder and Wells turbine PTO are equal to (3.1).

The mean absorbed power in regular waves is calculated as

$$P = \frac{C}{2\rho_{air}} |p_2 - p_1|^2 \quad (3.29)$$

where  $\rho_{air}$  is the equilibrium air density in both volumes.

### 3.3.2 Linear damper PTO between oscillating-body and fixed reference

In order to investigate benefits of alternative PTOs, an optimized linear spring-damper PTO model was developed for the compressible point absorber. For convenience, the equation of motion (3.1) is written in terms of the velocities  $u_3$  and  $u_7$ , which are related to the displacements  $\xi_3$  and  $\xi_r$ , in the frequency domain, as

$$u_3 = i\omega\xi_3 \quad u_r = i\omega\xi_r; \quad (3.30)$$

the resulting equation of motion is:

$$\left( i\omega \begin{bmatrix} M + m_{33} & m_{37} \\ m_{73} & m_{77} \end{bmatrix} + \begin{bmatrix} R_{33} & R_{37} \\ R_{73} & R_{77} \end{bmatrix} + \frac{1}{i\omega} \begin{bmatrix} k_{33} & k_{37} \\ k_{73} & k_{77} \end{bmatrix} \right) \begin{bmatrix} u_3 \\ u_r \end{bmatrix} = \begin{bmatrix} F_{e3} \\ F_{e7} \end{bmatrix}. \quad (3.31)$$

Equation (3.31) describes the dynamics of the compressible point absorber, but does not include the force exerted by the PTO. The equation of motion, including the PTO force  $F_p$ , can be written then in a more compact matrix form as:

$$Z_i u = F_e + F_p \quad (3.32)$$

where WEC intrinsic impedance  $Z_i$  is defined as

$$Z_i = \begin{bmatrix} Z_{i33} & Z_{i37} \\ Z_{i73} & Z_{i77} \end{bmatrix} = \begin{bmatrix} R_{33} + i \left( \omega (M + m_{33}) - \frac{\rho g S_2}{\omega} \right) & R_{37} + i \left( \omega m_{37} - \frac{\rho g S_1}{\omega} \right) \\ R_{73} + i \left( \omega m_{73} - \frac{\rho g S_1}{\omega} \right) & R_{77} + i \left( \omega m_{77} - \frac{\rho g S_1 + \frac{\gamma \rho_0}{v_0} S_1^2}{\omega} \right) \end{bmatrix} \quad (3.33)$$

and where

$$u = \begin{bmatrix} u_3 \\ u_r \end{bmatrix} \quad F_e = \begin{bmatrix} F_{e3} \\ F_{e7} \end{bmatrix} \quad F_p = \begin{bmatrix} F_{p3} \\ 0 \end{bmatrix} \quad (3.34)$$

The PTO force  $F_{p3}$  is assumed to be acting between a fixed reference (e.g sea bed) and the vertical cylinder with water plane area  $S_2 - S_1$  (it is not applied to the moving surface) as depicted in Fig. 3.2. It is described by using the PTO impedance  $Z_p$  as

$$F_{p3} = -Z_p u_3 = -(R_p + iX_p) u_3 \quad \text{with} \quad Z_p = R_p + iX_p, \quad (3.35)$$

where the  $R_p$  is the PTO damping (also known as resistance) and  $X_p$  is the PTO reactance.

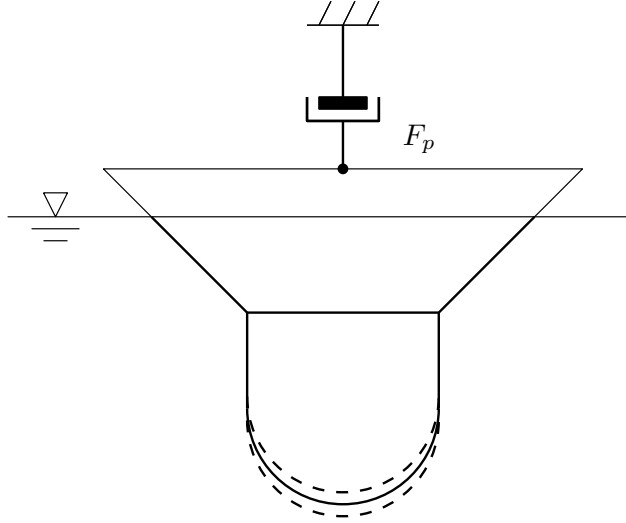


**Figure 3.2.** PTO configuration for compressible point absorber reacting against a fixed reference

With the definition of the PTO force by means of the PTO impedance as in (3.35), the average absorbed power is:

$$P = -\frac{1}{2}\text{Re}\{F_{p3}u_3^*\} = -\frac{1}{2}\text{Re}\{Z_p\}|u_3|^2 = -\frac{1}{2}R_p|u_3|^2. \quad (3.36)$$

Equation (3.36) shows that the resistive term of the PTO impedance (i.e.  $R_p$ ) is the one directly related to the power absorption, whereas the reactive part of the PTO impedance (i.e.  $X_p$ ) also affects power absorption, but in an indirect manner. In fact, the  $X_p$  affects the velocity  $u_3$  by altering the phase between the excitation force and the velocity itself, which indirectly affects the absorbed power in (3.36) through the term  $u_3$ .

### 3.3.2.1 Derivation of the optimal PTO impedance

In this section the objective is to derive the optimal PTO impedance when the PTO is applied between a fixed reference and the body. The first step is to write the PTO force in (3.35) in matrix form as

$$F_p = -\begin{bmatrix} Z_p & 0 \\ 0 & 0 \end{bmatrix} u. \quad (3.37)$$

The PTO in this form can then be substituted into the equation of motion (3.35)

$$\left( Z_i + \begin{bmatrix} Z_p & 0 \\ 0 & 0 \end{bmatrix} \right) u = F_e \quad (3.38)$$

and, by rearranging, the result is

$$u = \bar{Z}^{-1} F_e = \left( Z_i + \begin{bmatrix} Z_p & 0 \\ 0 & 0 \end{bmatrix} \right)^{-1} F_e. \quad (3.39)$$

The inverse of  $\bar{Z}_i$  can be written explicitly in terms of the elements of the intrinsic impedance ( $Z_{i,jk}$ ) and the PTO impedance ( $Z_p$ ) as

$$\bar{Z}^{-1} = \left( Z_i + \begin{bmatrix} Z_p & 0 \\ 0 & 0 \end{bmatrix} \right)^{-1} = \frac{1}{(Z_{i33} + Z_p) Z_{i77} - Z_{i37} Z_{i73}} \begin{bmatrix} Z_{i77} & -Z_{i37} \\ -Z_{i73} & (Z_{i33} + Z_p) \end{bmatrix} \quad (3.40)$$

The first element of the velocity vector  $u$ , that is the velocity of the body  $u_3$ , can be written explicitly as

$$\begin{aligned} u_3 = [1 \quad 0] u &= [1 \quad 0] \bar{Z}^{-1} F_e = \frac{Z_{i77} F_{e3} - Z_{i37} F_{e7}}{(Z_{i33} + Z_p) Z_{i77} - Z_{i37} Z_{i73}} \\ &= \frac{F_{e3}}{(Z_{i33} + Z_p) - \frac{Z_{i37} Z_{i73}}{Z_{i77}}} - \frac{F_{e7}}{\frac{(Z_{i33} + Z_p) Z_{i77}}{Z_{i37}} - Z_{i73}}. \end{aligned} \quad (3.41)$$

Using this expression and the definition in (3.36), the absorbed power becomes

$$P(Z_p) = -\frac{1}{2} R_p |u_3|^2 = -\frac{1}{2} R_p \left| \frac{F_{e3}}{(Z_{i33} + Z_p) - \frac{Z_{i37} Z_{i73}}{Z_{i77}}} - \frac{F_{e7}}{\frac{(Z_{i33} + Z_p) Z_{i77}}{Z_{i37}} - Z_{i73}} \right|^2. \quad (3.42)$$

The optimization of the PTO impedance can be carried out by maximizing (the absolute value of) equation (3.42) with respect to both the damping  $R_p$  and the reactance  $X_p$ .

If the objective is to optimize the damping only (i.e. passive control  $\Rightarrow X_p = 0$ ), then (3.42) becomes a function of  $R_p$ :

$$P(R_p) = -\frac{1}{2} R_p |u_3|^2 = -\frac{1}{2} R_p \left| \frac{F_{e3}}{(Z_{i33} + R_p) - \frac{Z_{i37} Z_{i73}}{Z_{i77}}} - \frac{F_{e7}}{\frac{(Z_{i33} + R_p) Z_{i77}}{Z_{i37}} - Z_{i73}} \right|^2. \quad (3.43)$$

and the optimal PTO resistance  $R_p^{opt}$ , for each frequency, is the solution of the one-dimensional optimization problem

$$R_p^{opt} = \arg \max_{R_p} -P(R_p). \quad (3.44)$$

It has to be noted that the solution of the optimization problem (3.44) is valid only for a specific frequency; therefore, the optimal PTO resistance is frequency dependent ( $R_p^{opt} = R_p^{opt}(\omega)$ ) and the optimization problem (3.44) has to be solved for all the frequencies of interest.

Additionally, it should also be noted that the absorbed power is larger when the PTO includes a reactive term, except for the resonance frequency, when they are equal. Therefore, equation (3.42) provides, in general, larger amount of power compared to equation (3.43), where the PTO is composed of the damping term only.

### 3.3.2.2 Analytical verification of optimal damping for stiff compression

When the compressible volume  $v_o$  becomes very small the stiffness of the compressible surface increases. In the limit case of  $v_o \rightarrow 0$  the WEC should behave as a rigid single-body device oscillating in heave. Thus, it is useful to calculate the limit

$$\lim_{k_{comp} \rightarrow +\infty} P = \lim_{k_{comp} \rightarrow +\infty} -\frac{1}{2} R_p \left| \frac{F_{e3}}{(Z_{i33} + Z_p) - \frac{Z_{i37} Z_{i73}}{Z_{i77}}} - \frac{F_{e7}}{\frac{(Z_{i33} + R_p) Z_{i77}}{Z_{i37}} - Z_{i73}} \right|^2. \quad (3.45)$$

and verify that it is equal to the power absorbed by a single-body point absorber in order to check the correctness of the equation of motion. It has to be noted that the equality is only a necessary condition (not sufficient) for the correctness of the equation of motion; that is, if the equality is not verified then the equation of motion is necessarily wrong. Conversely, if the equality is verified, the possibility of the equations of motion being wrong cannot be discarded. The first step is to define the damping and reactance terms of the elements of the intrinsic impedance matrix in (3.33) as

$$Z_{ijk} = R_{ijk} + iX_{ijk} \quad (3.46)$$

With this definition, it can be noted that the only term in which the spring term due to compressibility appears is  $X_{i77}$ , and that

$$\lim_{k_{comp} \rightarrow +\infty} X_{i77} = -\infty \quad (3.47)$$

Using (3.46) into the equation of the absorbed power in (3.43) and taking the limit

$$\begin{aligned}
P_\infty &= \lim_{k_{comp} \rightarrow +\infty} -\frac{1}{2} R_p \left| \frac{F_{e3}}{(Z_{i33} + Z_p) - \frac{Z_{i37} Z_{i73}}{Z_{i77}}} - \frac{F_{e7}}{\frac{(Z_{i33} + R_p) Z_{i77}}{Z_{i37}} - Z_{i73}} \right|^2 \\
&= \lim_{k_{comp} \rightarrow +\infty} -\frac{1}{2} R_p \left| \frac{F_{e3}}{(Z_{i33} + Z_p) - \frac{Z_{i37} Z_{i73}}{(R_{i77} + iX_{i77})}} - \frac{F_{e7}}{\frac{(Z_{i33} + R_p)(R_{i77} + iX_{i77})}{Z_{i37}} - Z_{i73}} \right|^2 \\
&= -\frac{1}{2} R_p \left| \frac{F_{e3}}{(Z_{i33} + Z_p) - 0} - 0 \right|^2 = -\frac{1}{2} R_p \left| \frac{F_{e3}}{(Z_{i33} + Z_p)} \right|^2
\end{aligned}$$

which is exactly the power absorbed by a single-body point absorber with a PTO impedance  $Z_p$ . It is known that the optimal PTO impedance for a single-DOF WEC is the complex-conjugate of the intrinsic impedance of the device [3]. In particular, by using the definition of the intrinsic impedance in (3.33), the optimal PTO impedance for a rigid body is:

$$Z_{P_{opt}} = R_{P_{opt}} + iX_{P_{opt}} = Z_{i33}^* = R_{33} - i \left( \omega (M + m_{33}) - \frac{\rho g S_2}{\omega} \right) \quad (3.48)$$

By substituting  $Z_{P_{opt}}$  into the absorbed  $P_\infty$ , the optimal absorbed power with infinite stiffness becomes

$$\begin{aligned}
P_{\infty_{opt}} &= -\frac{1}{2} R_{p_{opt}} \left| \frac{F_{e3}}{(Z_{i33} + Z_{P_{opt}})} \right|^2 = -\frac{1}{2} R_{33} \left| \frac{F_{e3}}{(Z_{i33} + Z_{i33}^*)} \right|^2 \\
&= -\frac{1}{2} R_{33} \left| \frac{F_{e3}}{\left( R_{33} + i \left( \omega (M + m_{33}) - \frac{\rho g S_2}{\omega} \right) + R_{33} - i \left( \omega (M + m_{33}) - \frac{\rho g S_2}{\omega} \right) \right)} \right|^2 \\
&= -\frac{1}{2} R_{33} \left| \frac{F_{e3}}{2R_{33}} \right|^2 = -\frac{|F_{e3}|^2}{8R_{33}} \quad (3.49)
\end{aligned}$$

The final expression in (3.49) is the optimal absorbed power of a rigid body WEC oscillating in one degree of freedom. Therefore, the necessary condition for the validity of the formula describing the optimal damping in (3.43) has been verified.

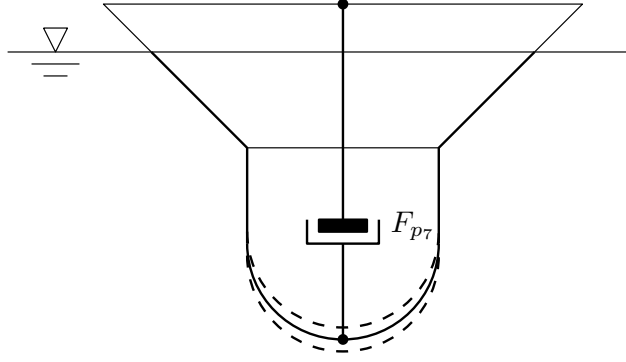


**Figure 3.3.** Self-reacting point absorber

### 3.3.3 Power absorption through the relative motion between the oscillating body and the compressible surface

In this section the PTO force ( $F_{p\tau}$ ) is assumed to be acting between the main structure of the oscillating body and the compressible surface, as depicted in Fig. 3.3. Following an analogous derivation as for the case described in section 3.3.2, the PTO force can be expressed in terms of the relative velocity of the compressible surface by means of the PTO impedance  $Z_p$  as

$$F_{p\tau} = -Z_p u_7 = -(R_p + iX_p) u_7 \quad \text{with} \quad Z_p = R_p + iX_p, \quad (3.50)$$

where, as already described in section 3.3.2, the  $R_p$  is the PTO damping and  $X_p$  is the PTO reactance. Thus, in the case of a self-reacting compressible point absorber, the average absorbed power is:

$$P = -\frac{1}{2} \text{Re} \{F_{p\tau} u_7^*\} = -\frac{1}{2} \text{Re} \{Z_p\} |u_7|^2 = -\frac{1}{2} R_p |u_7|^2. \quad (3.51)$$

#### 3.3.3.1 Derivation of the optimal PTO impedance

The procedure for the derivation of the optimal PTO impedance for the self-reacting point absorber is analogous to the derivation carried out for the WEC reacting against a fixed reference presented in section 3.3.2.1. The first step is to define the PTO force vector in matrix form as:

$$F_p = - \begin{bmatrix} 0 & 0 \\ 0 & Z_p \end{bmatrix} u. \quad (3.52)$$

Substituting of the above definition of the PTO force vector into the equation of motion (3.32) results in

$$\left( Z_i + \begin{bmatrix} 0 & 0 \\ 0 & Z_p \end{bmatrix} \right) u = F_e, \quad (3.53)$$

which, by solving for the velocity, is

$$u = \bar{Z}^{-1} F_e = \left( Z_i + \begin{bmatrix} 0 & 0 \\ 0 & Z_p \end{bmatrix} \right)^{-1} F_e = F_e. \quad (3.54)$$

In this case, the inverse of the matrix  $\bar{Z}_i$  can be written in terms of the elements of the matrix  $Z_i$  and the PTO impedance  $Z_p$  as

$$\bar{Z}^{-1} = \left( \begin{bmatrix} Z_{i33} & Z_{i37} \\ Z_{i73} & Z_{i77} \end{bmatrix} + \begin{bmatrix} 0 & 0 \\ 0 & Z_p \end{bmatrix} \right)^{-1} = \frac{1}{(Z_{i77} + Z_p) Z_{i33} - Z_{i37} + Z_{i73}} \begin{bmatrix} Z_{i77} + Z_p & -Z_{i37} \\ Z_{i73} & Z_{i33} \end{bmatrix} \quad (3.55)$$

The relative velocity of the compressible surface with respect to the main structure of the body,  $u_7$ , is the second element of the velocity vector; it can be written explicitly as

$$\begin{aligned} u_7 &= [0 \quad 1]u = [0 \quad 1]\bar{Z}^{-1}F_e = \frac{Z_{i33}F_{e7} - Z_{i73}F_{e3}}{(Z_{i77} + Z_p) Z_{i33} - Z_{i37} + Z_{i73}} \\ &= \frac{F_{e7}}{Z_{i77} + Z_p - \frac{Z_{i37}Z_{i73}}{Z_{i33}}} - \frac{F_{e3}}{(Z_{i77} + Z_p) \frac{Z_{i33}}{Z_{i73}} - Z_{i37}}. \end{aligned} \quad (3.56)$$

Finally, the expression of the absorbed power as function of the PTO impedance, defined as in (3.51), can be written as

$$P(Z_p) = -\frac{1}{2}R_p|u_7|^2 = -\frac{1}{2}R_p \left| \frac{F_{e7}}{Z_{i77} + Z_p - \frac{Z_{i37}Z_{i73}}{Z_{i33}}} - \frac{F_{e3}}{(Z_{i77} + Z_p) \frac{Z_{i33}}{Z_{i73}} - Z_{i37}} \right|^2 \quad (3.57)$$

Also in this case, if the PTO does not have a reactive component ( $X_p = 0$ ), then the absorbed power is

$$P(R_p) = -\frac{1}{2}R_p|u_7|^2 = -\frac{1}{2}R_p \left| \frac{F_{e7}}{Z_{i77} + R_p - \frac{Z_{i37}Z_{i73}}{Z_{i33}}} - \frac{F_{e3}}{(Z_{i77} + R_p) \frac{Z_{i33}}{Z_{i73}} - Z_{i37}} \right|^2, \quad (3.58)$$



and the optimal PTO resistance  $R_p^{opt}$ , for each frequency, is the solution of the one-dimensional optimization problem

$$R_p^{opt} = \arg \max_{R_p} -P(R_p). \quad (3.59)$$

As for the case of the point absorber reacting against a fixed reference, it should be noted that the solution of the optimization problem (3.59) is valid only for a specific frequency; therefore, the optimal PTO resistance is frequency dependent ( $R_p^{opt} = R_p^{opt}(\omega)$ ) and the optimization problem (3.59) has to be solved for all the frequencies of interest.

### 3.4 Available power density and absorption width

The absorption width  $d$  is calculated by dividing the mean absorbed power, defined in the previous sections, by the available wave power density,  $P_{avail}$ . The absorption width can be seen as the width of the wave-front that carries the same amount of power absorbed by the wave-energy converter. To better illustrate this concept, it is useful to first introduce the depth function as

$$D(kh) = \left[ 1 - \left( \frac{\omega^2}{gk} \right)^2 \right] kh + \frac{\omega^2}{gk} \quad (3.60)$$

where  $h$  is the water depth and  $k$  is the wave number, which is related to the wavelength  $\lambda$  as  $k = 2\pi/\lambda$ . A harmonic<sup>2</sup> planar<sup>3</sup> wave with angular frequency  $\omega$  and amplitude  $A$  transports, for a unit width of wave-front, an amount of power  $J$  equal to

$$J = \frac{\rho g^2 D(kh) |A|^2}{4\omega}. \quad (3.61)$$

The quantity  $J$  is generally known as *wave-energy transport* (also known as “wave-energy flux” or “wave-power flux”).

Water waves are dispersive, meaning that waves at different wavelengths travel at different speeds. In this case, the relation between the wave number and angular frequency is given by the dispersion relation

$$\omega^2 = gk \tanh(kh) \quad (3.62)$$

---

<sup>2</sup>A harmonic wave is a wave which varies sinusoidally in time and space

<sup>3</sup>A planar wave, also known as plane wave, is a wave for which the phase is constant on all the planes orthogonal to the direction of propagation.

When the water depth  $h$  is much larger than the wavelength  $\lambda$ , the quantity  $kh \gg 1$  and the depth function in (3.60) can be approximated as  $D(kh) \approx 1$ ; additionally, the dispersion relation simplifies to

$$\omega^2 = gk. \quad (3.63)$$

This condition ( $kh \gg 1$ ) is known as *deep-water*. By introducing the the wave period  $T$ , related to the angular frequency  $\omega$  as  $T = \frac{2}{\pi\omega}$ , and the wave height  $H$  defined as  $H = 2A$ , the average power density per unit wave-front carried by a harmonic plane wave in deep water is

$$J = \frac{\rho g^2 T H^2}{32\pi}. \quad (3.64)$$

# Chapter 4

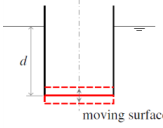
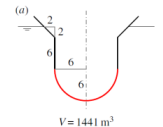
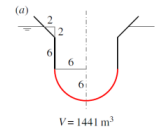
## Model-to-Model Comparison

Linear frequency domain models, based on the equations of motion described in Chapter 3, were coded using MATLAB scripts to compare results with those presented for several test cases using models developed in the UK study (REF). This model-to-model comparison, while not a rigorous model validation, provides quality control and quality assurance (QA/QC) that the present study's model was implemented correctly. All coefficients for the equations of motion were independently derived using the radiation-diffraction model, NEMOH [1], as described in Chapter 2.

Several test cases are modeled, including the compressible heaving cylinder, a compressible point absorber with a Wells turbine PTO, and one with a linear PTO. Information on the PTO, CDOF, and design parameters are summarized in Table 4.1. Results from these compressible point absorber simulations were compared to an equivalent rigid point absorber with the same shape and mass.

Plots of heave displacement per incident wave amplitude as a function of angular frequency show the degree to which the CDOF benefits body response performance by lowering the natural resonance frequency and broadening its resonance bandwidth relative to the equivalent rigid point absorber (no CDOF). As shown in Figs. 4.1, 4.2, and 4.4, plots generated from the present study's models are identical to those from the UK study. The CDOF lowers the natural resonance frequency for all test cases relative to the value predicted for the rigid point absorber. It also broadens the resonance bandwidth relative to the bandwidth predicted for the rigid point absorber. The magnitude of these benefits depends on the initial compressible volume of the CDOF.

Figures 4.3 and 4.5 depict the power absorption as a function of wave period [8]; these plots are used to evaluate power performance gained by the CDOF relative to the equivalent rigid point absorber (no CDOF). In these plots power absorption width is determined by normalizing the mechanical power extracted from the PTO by the wave power. The plots include the theoretical maximum limit of power absorption width for a heaving symmetrical body [3] (p.216). This theoretical limit is an additional verification of the model by delineating the upper bound of power absorption width.

Device	PTO	CDOF	Test Cases	Results
Heaving Cylinder 	None	Compressible volume with downward facing moving surface	Rigid cylinder, and CDOF with two compressible volumes, $V_{10} = 1000 \text{ \& } 1500m^3$	Fig. 4.1
Heaving absorber 	Wells air turbine with $C = 0.02m^2 - s$	Compressible volume $V_{10} = 1441m^3$ with downward facing horizontal moving surface	CDOF with three fixed auxiliary volumes, $V_{20} = 2000, 3000, \text{ \& } 4000m^3$	Fig. 4.2, Fig. 4.3
Heaving absorber 	Wells air turbine with $C = 0.02m^2 - s$ and linear damper PTO with $R_p = 3 \times 10^5 kg/s$	Compressible volume $V_{10} = 1000m^3$ with downward facing horizontal moving surface	Rigid absorber and compressible absorber with fixed auxiliary volume, $V_{20} = 1000m^3$	Fig. 4.4, Fig. 4.5

**Table 4.1.** Test cases for model-to-model comparison

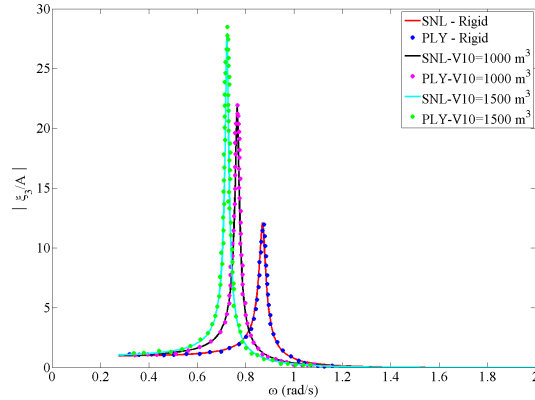


**Figure 4.1.** Model to model comparison for response of heaving compressible cylinder test cases with varying compressible volumes compared to rigid cylinder.

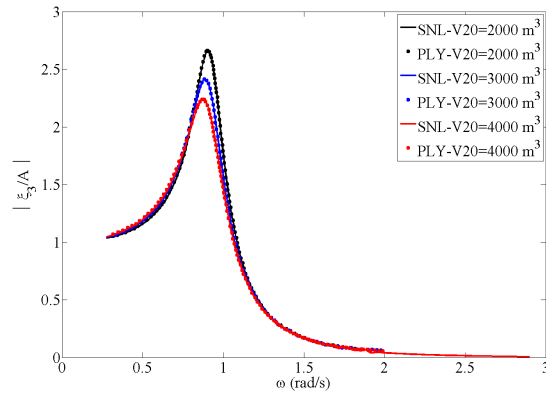


**Figure 4.2.** Model to model comparison for response of heaving point absorber test cases with varying compressible volumes.

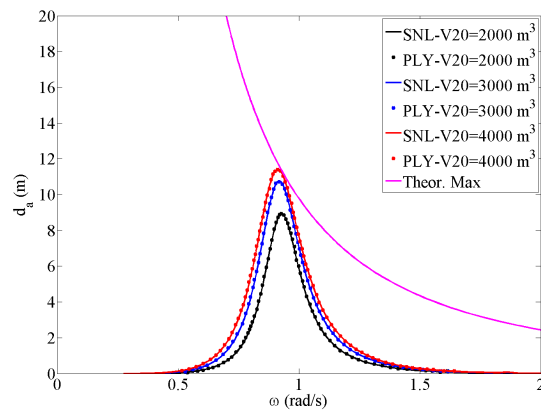


**Figure 4.3.** Model to model comparison for energy capture of heaving point absorber test cases with varying compressible volumes. The theoretical maximum energy capture width is  $\lambda/2\pi$

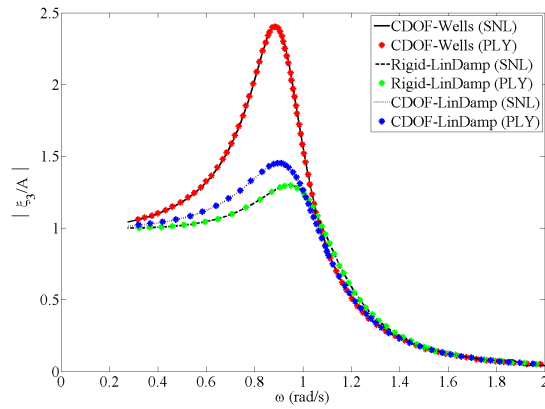


**Figure 4.4.** Model to model comparison for response of heaving point absorber test cases comparing rigid absorber with linear damper PTO to compressible absorber with Wells turbine PTO, and compressible absorber with linear damper PTO.

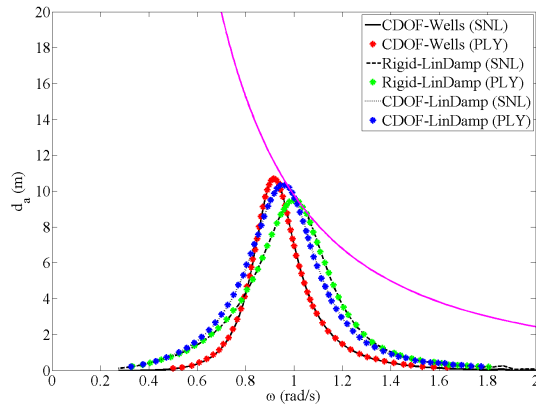


**Figure 4.5.** Model to model comparison for energy capture of heaving point absorber test cases comparing rigid point absorber with linear damper PTO to compressible absorber with Wells turbine PTO, and compressible absorber with linear damper PTO. The theoretical maximum energy capture width is  $\lambda/2\pi$

# Chapter 5

## Optimized PTO Heave and Absorption Width

In this section the simulation results are reported for two types of compressible point absorbers. Section 5.1 includes a description of the simulation results for a compressible point absorber reacting against a fixed reference. A self-reacting compressible point absorber is considered in section 5.2. In both cases the simulation results are compared against a rigid point absorber of the same shape and physical dimensions.

### 5.1 Compressible point absorber reacting against a fixed reference

The simulation results reported in this section refer to the point absorber depicted in Figure 3.2, where power absorption is carried out by means of a linear damper connected between the main structure of the point absorber and a fixed reference (e.g. the seabed). The amount of power absorbed by the point absorber depends on the value of the linear damping; the optimal damping is the value which maximizes the absorbed power. The optimal damping is dependent on the period of the incoming wave and, for each period, it is calculated by solving the optimization problem described in section 3.3.2.1 (see eq. (3.44)).

Figure 5.1 shows the average absorbed power as function of the wave period for an incident wave with amplitude equal to  $A = 1m$ , for both the rigid body and the compressible point absorber. It can be noted immediately that the rigid body point absorber can absorb the maximum amount of power available, given by eq. (3.64), if using complex conjugate control<sup>1</sup> [3](p. 206). Resistive control, on the other hand, only allows maximum absorption at resonance, that is, when the period of the incident wave  $T$  is equal to the resonance period, that is  $T = T_{res} = 6.1s$ . Two additional curves are plotted in the same figure, corresponding

---

<sup>1</sup>Complex conjugate control is a control strategy, the objective of which is to make the device resonate at all frequencies. The name is derived from the form in which the controller is specified: If the control law is written as function of body velocity multiplied to a term named “PTO impedance”, then the valued of the PTO impedance that maximizes the absorbed power is equal to the complex conjugate of the device intrinsic impedance. As an example, section 3.3.2 provides a mathematical description of the PTO impedance and the intrinsic impedance for a point absorber with CDOF.

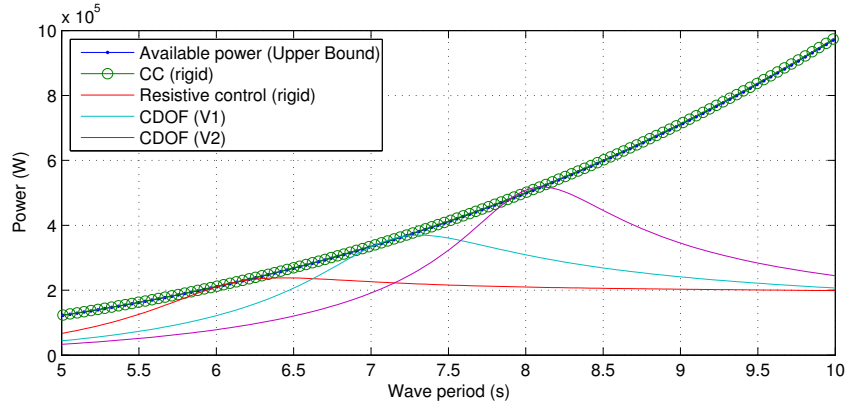


**Figure 5.1.** Average absorbed power as function of the wave period for waves with amplitude  $A = 1m$

to the power absorbed by the compressible point absorber for two different values of the stiffness coefficient associated to the compressible mode of motion. The stiffness coefficients, in turn, correspond to different values of the compressible volume, which are<sup>2</sup>  $V1 = 5 \cdot 10^3 m^3$  and  $V2 = 2 \cdot 10^4 m^3$ .

Figure 5.1 clearly shows one of the benefits provided by a compressible point absorber when compared to a rigid one, which is that it can be tuned to different wave periods by changing the amount of compressible volume<sup>3</sup>. For a compressible volume equal to  $V1$ , the resonance period of the device has shifted from  $T_{res} = 6.1s$  to  $T_{res}^{V1} = 7.3s$ , and the amount of average power absorbed by the compressible point absorber is equal to the upper bound<sup>4</sup>. For a compressible volume equal to  $V2$ , the resonance period is shifted to  $T_{res}^{V2} = 8.1s$ .

It has to be noted that the resonance period of the device can also be altered by allowing the PTO to include a spring term. However, this would require the PTO to use reactive power and, most importantly, by adding a spring term to the PTO, the resonance period can only be decreased. It can be shown by examining the equation of motion of the device that the PTO stiffness would be added to the hydrostatic stiffness, with the consequence of stiffening the device, thus resulting in a higher resonance frequency<sup>5</sup> (lower resonance period).

Comparing Figure 5.1 with Figure 5.2, reveals an additional benefit provided by the compressible degree of freedom. Figure 5.2 shows the peak power flowing through the PTO for

<sup>2</sup>The value of the compressible volumes are quite large; however, this is of no concern because the same stiffness coefficient can be implemented using other mechanisms

<sup>3</sup>the compressible volume can be adjusted by opening/closing internal chambers to the point absorber, for example. More generally, however, the compressible point absorber can be tuned by acting on the stiffness coefficient of the compressible surface

<sup>4</sup>which is, in turn, equal to the amount of power absorbed by the rigid-body point absorber when controlled using the complex conjugate strategy

<sup>5</sup>The objective is to allow smaller devices to resonate at longer periods, i.e. lower frequencies



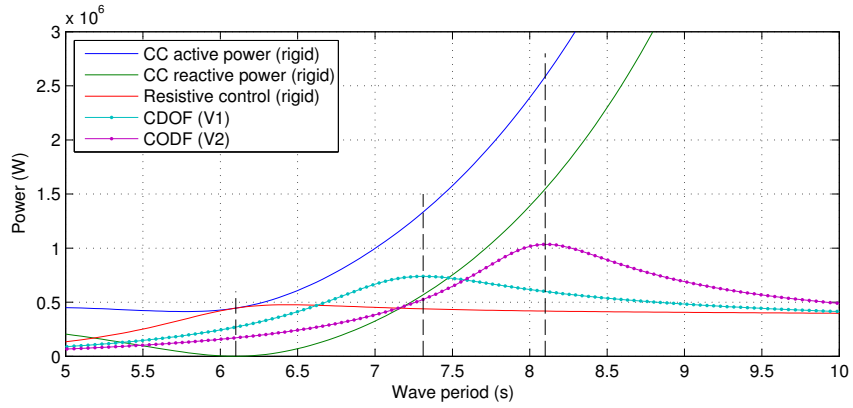


**Figure 5.2.** Peak power flowing through the PTO as function of the wave period for waves with amplitude  $A = 1m$

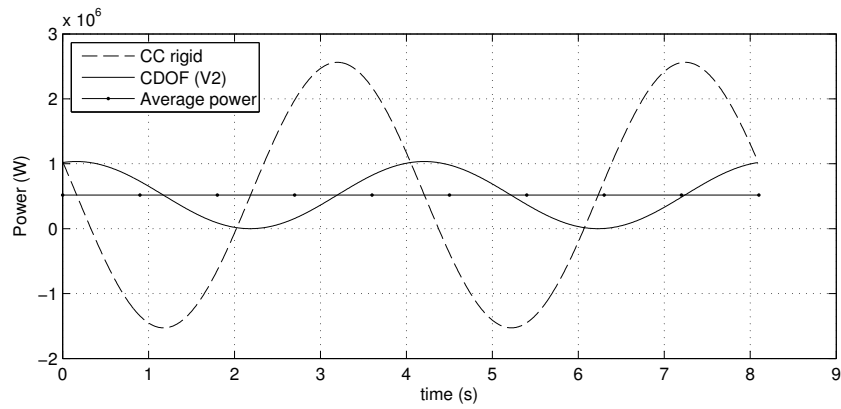


**Figure 5.3.** Time profile of the power flowing through the PTO for an incident wave with period  $T = 8.1s$  and amplitude  $A = 1m$

the rigid body when using both complex conjugate control and resistive control. Additionally, this same figure shows the peak power through the PTO of a compressible point absorber. The quantities plotted in Figure 5.2 can be better understood by examining Figure 5.3, which shows the time profile of the instantaneous power flowing through the PTO of a rigid point absorber controlled using complex conjugate control (solid line), and the power flowing through the PTO of a compressible point absorber (dashed line). In this case, the wave period is  $T = 8.1s$  and the wave amplitude is  $A = 1m$ . The points on the blue curve in Figure 5.2, for each wave period, correspond to the maximum positive value of dashed line in Figure 5.3, whereas the points on the green line in Figure 5.2, for each wave period, correspond to the maximum negative value of the dashed line in Figure 5.3 (peak value of the reactive power).

Comparing Figure 5.1 with Figure 5.2 shows that, for wave periods larger than the natural resonance period ( $T > T_{res}$ ), the compressible point absorber can use a smaller PTO to absorb the same amount of average power as the rigid point absorber using the complex conjugate strategy<sup>6</sup> if the stiffness terms are tuned appropriately. For example, when the period of the incident wave is  $T = 7.3s$ , Figure 5.1 shows that the absorbed power of both the rigid point absorber and the compressible point absorber ( $V1$ ) is  $P_{avg} = 3.8 \cdot 10^5 W$ . However, Figure 5.2 shows that the the maximum amount of power flowing through the PTO of the rigid point absorber (blue line) is approximately 1.5 time larger than the maximum power flowing through the PTO of the compressible point absorber.

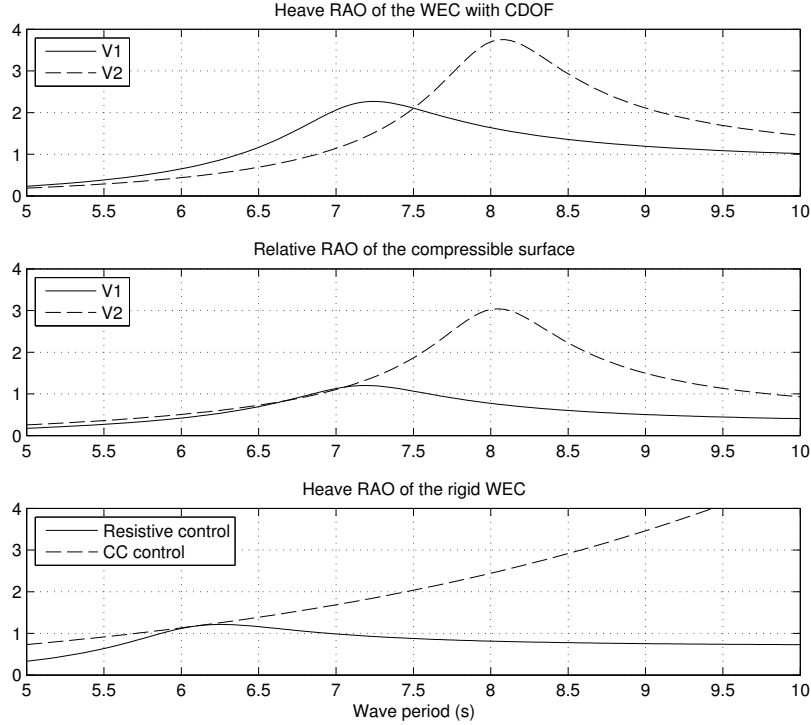
The difference in peak power is even larger for longer wave periods. In fact, when the compressible volume is equal to  $V2$ , Figure 5.2 shows that the peak power flowing through the PTO of the rigid point absorber is approximately 2.5 times larger than the power flowing through the PTO of the compressible point absorber. This implies that, in order to absorb the same amount of power, the rigid point absorber requires a PTO with power rating 2.5 times larger than the PTO of the compressible point absorber. Figure 5.3 illustrates this concepts even more clearly: the dashed sinusoid is the instantaneous power flowing through the PTO of the rigid point absorber, whereas the solid sinusoid is the instantaneous power flowing through PTO of a compressible point absorber. In both cases the average absorbed power is the same (solid line with “dot” markers), but the dashed sinusoid (rigid point absorber) is 2.5 times larger than the solid sinusoid (compressible point absorber).

Figure 5.3 also shows that a compressible point absorber does not require reactive power, as the solid sinusoid is never negative. This fact is extremely important when designing the PTO. It has been shown in [4] that when the PTO is required to generate reactive power it must have a very high efficiency, otherwise the loss in power can be so large as to completely counteract the benefits of implementing complex conjugate control. As a consequence, a compressible point absorber will allow a PTO which is both smaller (smaller power rating), and with less stringent requirements on its efficiency, thus allowing a considerable reduction in cost.

As a final consideration, it is worth noting that Figure 5.2 also shows that, at the natural

---

<sup>6</sup>that is equal to the upper bound of the available power



**Figure 5.4.** Response Amplitude Operator (RAO) of the WEC and compressible surface

resonance period of the rigid point absorber ( $T_{res} = 6.1s$ ), the peak active power when implementing CC control (blue curve) is equal to the peak power when implementing resistive control (red curve); in other words, the amount of reactive power at resonance is zero (green curve)<sup>7</sup>.

The motion of the devices and of the compressible surface are plotted in Figure 5.4; in particular, the top two plots show the Response Amplitude Operator<sup>8</sup> (RAO). This figure shows that, in order for the compressible point absorber to achieve the absorption performance previously described, there is a price to pay in terms of oscillation amplitude. In fact, the RAOs of both the main structure of the compressible point absorber (top plot) and the compressible surface (middle plot) are larger than the oscillation amplitude of the rigid point absorber controlled using the complex control strategy (dashed line in the bottom plot).

<sup>7</sup>this is a well known fact in the theory of linear oscillating systems; it has been added for completeness

<sup>8</sup>The RAO is the amplitude of the motion normalized with respect to the wave amplitude

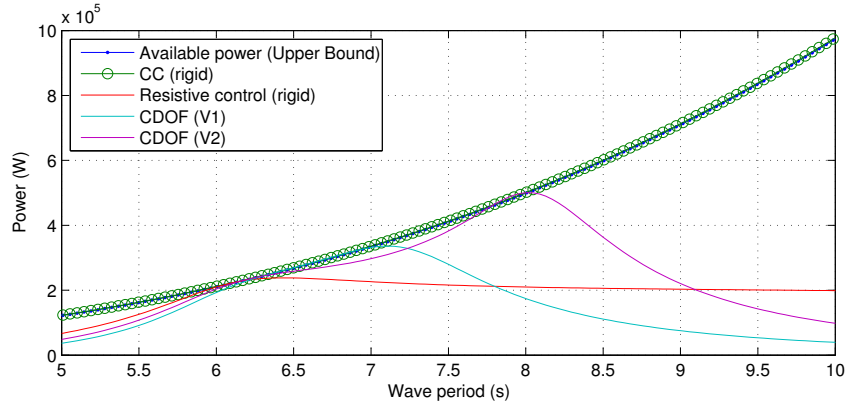


**Figure 5.5.** Average absorbed power as function of the wave period for waves with amplitude  $A = 1m$

## 5.2 Self-reacting Point Absorber

In this section the simulation results refer to the point absorber depicted in Figure 3.3. For this device, the same considerations on power absorption apply as for the compressible point absorber reacting against a fixed reference described in sec. 5.1 with one notable difference; as shown in Figure 5.5 the self-reacting compressible point absorber is capable of absorbing power on a broader frequency band compared to the compressible point absorber reacting against a fixed reference. The power absorption curve of the compressible point absorber, when the volume equal to  $V_2$ , nearly reaches the upper bound of the power absorption (green line marked with circles) for a large interval of wave periods ( $6s < T < 8s$ ). This behavior is highlighted in Figure 5.9, which depicts the capture ratio, that is the ratio between the average absorbed power and the available power in the wave (see eq. (3.64)). This same figure also includes the average absorbed power of the rigid point absorber using resistive control (blue line), of the compressible point absorber reacting against a fixed reference (black solid line), and of the self-reacting compressible point absorber. The absorption characteristics of the self-reacting compressible point absorber shows two distinct resonances, one at (or close to) the natural resonance of the rigid body ( $T_{res} = 6.1s$ ), and the second one at the resonance period of the compressible point absorber reacting against a fixed reference. For wave periods in the interval between the two resonances the capture ratio is close to one, meaning that the device is capable of absorbing a near optimum amount of power.

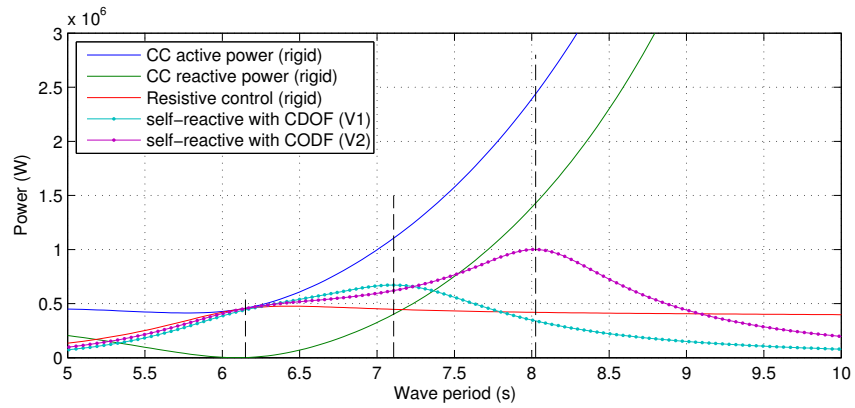


**Figure 5.6.** Peak power through the PTO as function of the wave period for waves with amplitude  $A = 1m$

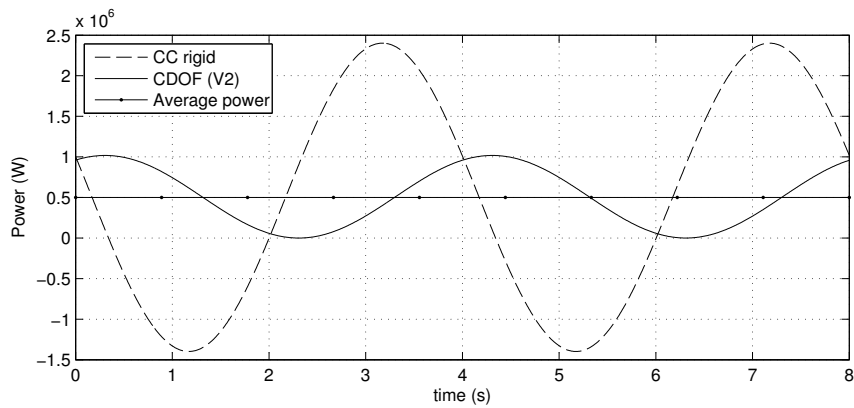


**Figure 5.7.** Time profile of the power flowing through the PTO for an incident wave with period  $T = 8s$  and amplitude  $A = 1m$

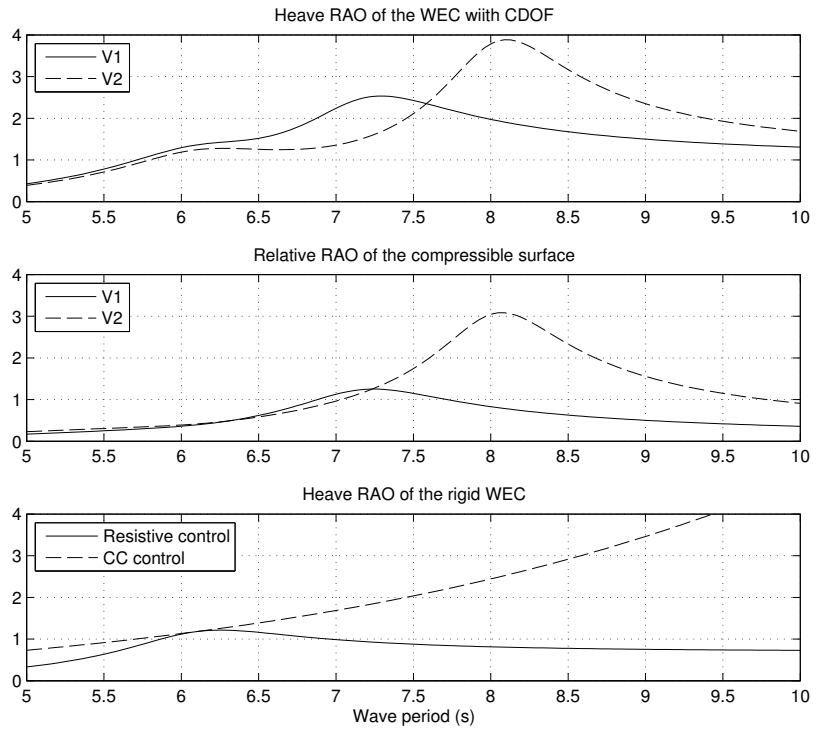


**Figure 5.8.** Response Amplitude Operator (RAO) of the WEC and compressible surface

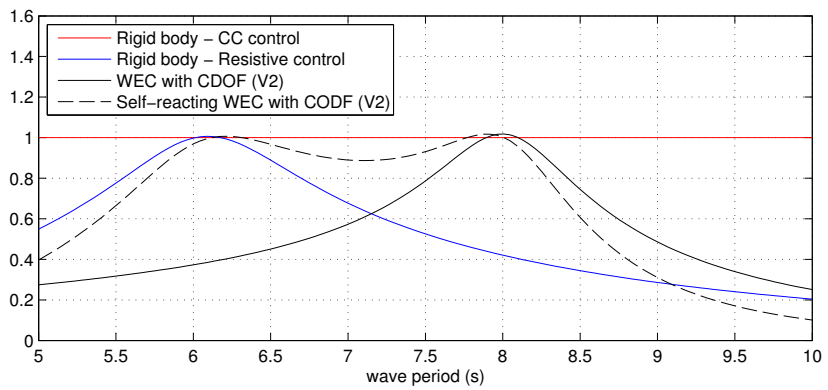


**Figure 5.9.** Comparison of capture ratios, defined as absorbed power divided by available power in eq. (3.64)

# Chapter 6

## Conclusions

The main objective of this study is to analyze the effects of a compressible degree of freedom (CDOF) on power absorption for point absorbers. The model of a compressible point absorber, which includes a CDOF, is derived first, and compared against the study presented by Kurniawan et al. in [8]. Subsequently, the damping of the PTO is optimized for two configurations of the device: a point absorber in which the PTO is placed between the main body of the WEC and a fixed reference (e.g. the seabed), and a self-reacting point absorber, in which the PTO is placed between the main body of the point absorber and the compressible surface. The PTO damping is optimized by means of a numerical procedure; however, an asymptotic analysis is also carried out which shows agreement with the known theoretical results.

The present study demonstrates that a compressible point absorber, with a passive PTO and optimized damping, can also achieve at the same performance levels or better than an optimally controlled rigid point absorber using reactive power from the PTO. The simulation results show that a compressible point absorber, with a passive PTO and optimized damping, can also achieve at the same performance levels or better than an optimally controlled rigid point absorber using reactive power from the PTO. The rigid point absorber used for the comparison has the same shape and mass.

Eliminating the need for a reactive PTO could be a game changer for the WEC industry. It would substantially reduce costs by reducing PTO design complexity and power rating. In addition, it would negate the adverse effects of reactive PTO efficiencies on absorbed power demonstrated by Genest et al. [4], who show that the theoretical performance gains of optimal reactive control to increase absorbed power, even with a 90% PTO efficiency, is reduced by 60% due to energy losses incurred when transferring large amounts of power for control bi-directionally from the floating body to the PTO. For PTO efficiencies below 50%, Genest et al. conclude that reactive control becomes useless. Additionally, the self-reacting point absorber with CDOF shows the capability to absorb power over a broader frequency range compared to the point absorber with CDOF reacting against a fixed reference.

Theoretical analysis and simulation results in the present study show that the improvement in performance requires large compressible volumes and large oscillations of the compressible surface. These are practical limitations that need to be addressed with further research; especially for low frequencies. All compressible volumes exceed the submerged volume of the point absorber by significant amounts; requiring auxiliary compressible volume

storage units that are connected to the air chamber in the submerged portion of the point absorber. While realistic, these auxiliary units would increase the CapEx and OpEx costs, potentially reducing the aforementioned benefits gained by CDOF.

A potential direction of research for the mitigation of the large compressible volume requirements is the implementation of the stiffness of the compressible surface by means of a different mechanical device. Additionally, the hydrodynamic properties of the device affect both the compressible volume requirements and the motion of the compressible surface; both of these drawbacks can be addressed by optimizing the shape of the device. The optimization can be carried out with the objective to optimize the overall cost, rather than focusing solely on power absorption. Future research should also focus on laboratory-scale physical model studies, to provide more rigorous model verification and validation.



# References

- [1] NEMOH, available: Available: <http://lhea.ec-nantes.fr/doku.php/emo/nemoh/start>.
- [2] WAMIT, available: <http://www.wamit.com/index.htm>.
- [3] Johannes Falnes. *Ocean Waves and Oscillating Systems*. Cambridge University Press, Cambridge; New York, 2002.
- [4] Romain Genest, Flicien Bonnefoy, Alain H. Clment, and Aurlien Babarit. Effect of non-ideal power take-off on the energy absorption of a reactively controlled one degree of freedom wave energy converter. *Applied Ocean Research*, 48:236 – 243, 2014.
- [5] Haberman. *Basic physics of fluid damper*. 2014.
- [6] R. Haberman. The bobbing cylinder with a compressible volume: thoughts on fluid mass and stiffness. 2014.
- [7] J. Journee and W. Massie. *Offshore Hydromechanics*. Delft University of Technology, 2001.
- [8] Adi Kurniawan, Deborah Greaves, and John Chaplin. Wave energy devices with compressible volumes. *Proceedings of the Royal Society of London A: Mathematical, Physical and Engineering Sciences*, 470(2172), 2014.
- [9] J.N. Newman. Wave effects on deformable bodies. *Applied Ocean Research*, 16(1):47 – 59, 1994.
- [10] Francis T. Ogilvie. Recent progress towards the understanding and prediction of ship motions. In *Proceedings of the 6<sup>th</sup> Symposium on Naval Hydrodynamics*, Washington DC, 1964.
- [11] Z. Yu and J. Falnes. State-space modelling of a vertical cylinder in heave. *Applied Ocean Research*, 17(5):265 – 275, 1995.

## DISTRIBUTION:

- 1 MS 0899 Technical Library, 9536 (electronic copy)



